Inorganica Chimica Acta 557 (2023) 121715

Contents lists available at ScienceDirect

Inorganica Chimica Acta

journal homepage: www.elsevier.com/locate/ica

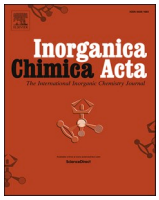

Complexes of 1,10-phenanthroline-mono-*N*-oxides with copper(II) and nickel(II) in aqueous solution and solid phase

Norbert Lihi [a,*], Nóra V. May [b], Antal Udvardy [c], Ferenc Najóczki [d,e], Dóra Bonczidai-Kelemen [d,e], Róbert Diószegi [d,e], Dóra Szalóki [a], Szófia O. Sánta [e], István Fábián [a,*]

[a] *ELKH-DE Mechanisms of Complex Homogeneous and Heterogeneous Chemical Reactions Research Group, Department of Inorganic and Analytical Chemistry, University of Debrecen, Debrecen H-4032, Hungary*
[b] *Centre for Structural Sciences, Research Centre for Natural Sciences, Budapest H-1117, Hungary*
[c] *Department of Physical Chemistry, University of Debrecen, Debrecen H-4032, Hungary*
[d] *Doctoral School of Chemistry, University of Debrecen, Debrecen H-4032, Hungary*
[e] *Department of Inorganic and Analytical Chemistry, University of Debrecen, Debrecen H-4032, Hungary*

ARTICLE INFO

Keywords:
Phenanthroline-*N*-oxides
Copper(II)
Nickel(II)
Stability
Structure

ABSTRACT

Thorough equilibrium and spectroscopic studies are reported on the complexes formed between copper(II) or nickel(II) and derivatives of phenanthroline-mono-*N*-oxides (1,10-phenanthroline-1-*N*-oxide (phenO), 2,9-dimethyl-1,10-phenanthroline-1-*N*-oxide (DMPO) and 3,4,7,8-tetramethyl-1,10-phenanthroline-1-*N*-oxide (TMPO)). PhenO exhibits excellent metal binding ability, both copper(II) and nickel(II) form bis complexes in which the ligands coordinate to the metal ions via the (N,O) donor set. In the case of copper(II), a square-pyramidal complex forms, where the phenO-s coordinate at the corners of the square and the remaining site is occupied by the water molecule. The bis complex formed between nickel(II) and phenO possesses square-planar geometry in solution, however, the Ni(II) ion exhibits a distorted octahedral geometry in solid phase. DMPO forms relatively stable complexes with copper(II), but the coordination of this ligand to nickel(II) could not be confirmed. Because of precipitate formation in the entire studied pH range (pH = 2.0 – 11.0), well defined complexes could not be identified in the copper(II) – TMPO system. In contrast, this ligand forms stable water soluble nickel(II) complexes. The noted selectivity of these ligands in complex formation reactions is explained by considering the plasticity of copper(II), the rigid, square-planar geometry of nickel(II) and the enhanced steric repulsion of the methyl substituents of DMPO.

1. Introduction

1,10-Phenanthroline (phen) and its substituted derivatives are among the most common and frequently used metal ion binding bidentate ligands that form stable complexes with transition metal ions. Therefore, a large number of studies have been reported on the coordination chemistry and applications of phenanthroline – metal ion complexes.[1] Moreover, the importance of an inexhaustible number of ternary phenanthroline complexes has been shown in a great variety of applications. The oxidation of phenanthroline and its derivatives yields the corresponding phenanthroline-*N*-oxides (phenO-s). These compounds are the subject of interest due to their widespread possible applications in organic chemistry (phase transfer catalysis, cycloaddition reactions, organocatalysis, etc.).[2–4] Earlier studies implied that the oxidation of phen-s is not a trivial task and vigorous experimental procedures are required to yield the corresponding phenO-s. Recently, we have confirmed that phen-s can readily be oxidized to *N*-oxides by Oxone ($KHSO_5$) under relatively mild conditions in aqueous solution and we have developed a method to synthesize a series of 1,10-phenanthroline-*N*-oxides. The crucial point in the synthesis is the use of appropriate pH.[5,6] Under acidic conditions, the reaction yields mono-*N*-oxides which feature a strong intramolecular hydrogen bond in protonated form that prevents the oxidation of the second nitrogen atom. In contrast to phenanthroline and its derivatives, only very limited information is available on the coordination chemistry of the corresponding mono-*N*-oxides. [7–9].

The coordination chemistry of these new compounds is an intriguing issue considering that they most likely form six-membered chelates with

* Corresponding authors.
E-mail addresses: lihi.norbert@science.unideb.hu (N. Lihi), ifabian@science.unideb.hu (I. Fábián).

https://doi.org/10.1016/j.ica.2023.121715
Received 3 May 2023; Received in revised form 1 August 2023; Accepted 6 August 2023
Available online 8 August 2023

the metal ion which is a less favorable coordination mode compared to the five-membered chelates. Consequently, the formation of less stable complexes are anticipated with phenO-s compared to phen-s, and the strictly planar *N*-aromatic rings of the ligand may also be also distorted in the phenO complexes. These characteristics are expected to be associated with specific electronic, redox and reactivity patterns.

Now we report a detailed equilibrium, spectroscopic (UV–vis, EPR, MS and X-Ray) and computational (DFT) study on the complex formation reactions between copper(II) and nickel(II) and the following ligands: 1,10-phenanthroline-mono-*N*-oxide (phenO), 2,9-dimethyl-1,10-phenanthroline-mono-*N*-oxide (DMPO) and 3,4,7,8-tetrametil-1,10-phenanthroline-mono-*N*-oxide (TMPO) (Scheme 1). The coordination chemistry of the selected metal ions has thoroughly been described earlier and the literature results offer a plausible possibility to benchmark the features of the new complexes. The results provide deep insight into the equilibrium, structural and spectroscopic properties of these coordination compounds and also make possible to analyze the role of the methyl-substituents in the complex formation processes. The results may also be useful to explore how these novel metal complexes can be utilized in different fields of chemistry.

2. Experimental section

2.1. Materials

The phenanthroline derivatives, phen (1,10-phenanthroline), DMP (2,9-dimethyl-1,10-phenanthroline) as well as TMP (3,4,7,8-tetrametil-1,10-phenanthroline) were purchased from Merck Co. (Budapest, HU) and used without further purifications. phenO, DMPO and TMPO were synthetized using the corresponding phenanthroline derivates and (peroxomonosulphate-ion (HSO_5^-) under acidic condition and were identified by their ^{1}H NMR and mass spectra as described earlier. [6,10] Details of the synthesis are provided in the Supporting Information (SI). Potassium peroxomonosulfate (PMS) is available as a stable triple salt, brand named Oxone ($2KHSO_5{\cdot}KHSO_4{\cdot}K_2SO_4$, Merck) and the solid was added directly to the reaction mixtures during the synthesis. All the chemicals and solvents used for synthetic purposes were purchased from commercial sources in the highest available purity and used without further purifications. The concentration and the purity of phenO and its derivates were determined by pH-potentiometric titrations. The stock solutions of $NiCl_2$ and $CuCl_2$ were prepared from analytical reagents (≥99.95%; VWR Int.) and their concentrations were determined by complexometric titrations with EDTA. For solution equilibrium and spectroscopic studies, triple de-ionized and ultrafiltered (Millipore Milli-Q system) water was used.

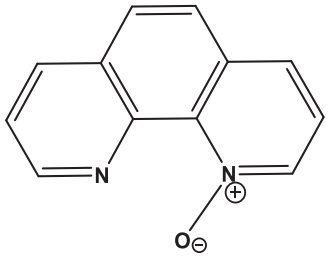

phenO: 1,10-phenanthroline-mono-N-oxide

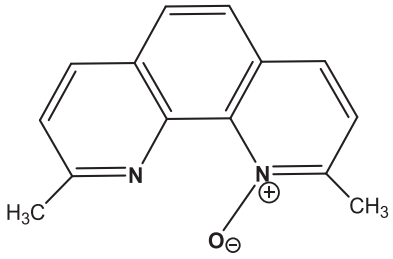

DMPO: 2,9-dimethyl-1,10-phenanthroline-mono-N-oxide

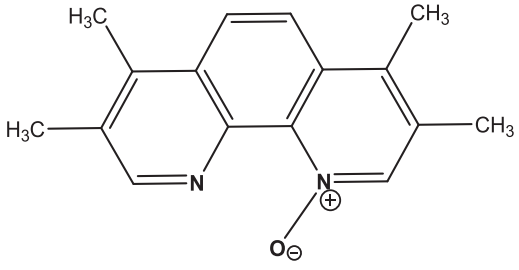

TMPO: 3,4,7,8-tetramethyl-1,10-phenanthroline-mono-N-oxide

Scheme 1. The phenanthroline-mono-*N*-oxides used in this study.

2.2. pH-potentiometry

The protonation constants ($\log K_i$) of the ligands and the overall stability constants ($\log\beta_{pqr}$) were determined by pH-potentiometric titration method. In these titrations, 10 mL aliquots of the ligands (ca. 3.0 mM) were titrated with carbonate-free potassium-hydroxide solution (0.5 M), and the metal-to-ligand ratio was varied between 1:1, 1:2 and 1:3. The ionic strength of the samples was adjusted to 0.2 M with KCl, and the measurements were carried out at 25 °C. The samples were stirred using a magnetic stirrer (Metrohm). pH measurements were made using a Metrohm 785 DMP Titrando pH-meter equipped with a 6.0234.100 combination glass electrode (Metrohm). The pH readings were converted to hydrogen ion concentrations as described by Irving et al., and $pH = -\lg[H^+]$.[11] Protonation constants and the overall stability constants, $\beta_{pqr} = [M_pL_qH_r]/[M]^p[L]^q[H]^r$ of the nickel(II), or copper(II) complexes (charges are omitted for the sake of simplicity) were calculated by using the designated softwares, PSEQUAD [12] and SUPERQUAD [13].

2.3. Spectroscopic measurements

UV − visible spectra of the complexes were recorded with an Agilent Technologies UV–vis Cary 60 scanning spectrophotometer in the 300–800 nm wavelength range using the same concentration range as in the pH-potentiometric titrations. Steady-state fluorescence measurements were carried out using a Jasco FP-8500 spectrofluorometer equipped with a Xe lamp light source. Emission spectra were recorded at 25 °C, using a 2.5 nm excitation and 2.5 nm emission bandwidth and 100 nm/min scanning speed. Fluorescence lifetimes of the phenanthroline-*N*-oxides were determined by laser flash photolysis. These experiments were carried out in an Applied Photophysics LKS.60 ns transient absorption spectrometer, equipped with a Quantel Brilliant Nd:YAG laser (1064 nm). The third harmonic generator was used which emits at 355 nm. For parameter fitting to the experimental data, the controlling software of the spectrometer was used.

2.4. Relaxometry

Measurements of longitudinal (T_1) and transversal (T_2) relaxation times were performed by using a Bruker Minispec MQ-20 NMR analyzer working at 0.49 T (proton Larmor frequency). The temperature of the sample holder was set (25.0 ± 0.2 °C) and controlled with the use of a circulating water bath. The T_1 values were determined with the inversion recovery method (180° –τ – 90°) by averaging 4–6 data points obtained at 10 different τ delay values. The transverse relaxation times (T_2) were measured by using the Carr-Purcell-Meiboom-Gill sequence (CPMG) sequence by averaging again 4–6 data points. The T_1 and T_2 relaxivities of the complexes were determined using the same concentration range as in the pH-potentiometric titrations.

2.5. Mass spectrometry

ESI-TOF-MS measurements were carried out with a Bruker maXis II MicroTOF-Q type Qq-TOF-MS instrument (Bruker Daltonik, Bremen, Germany) in positive mode. The instrument was equipped with an electrospray ion source where the spray voltage was 4 kV. N_2 was utilized as a drying gas and the drying temperature was 200 °C. The spectra were accumulated and recorded using a digitalizer at a sampling rate of 2 GHz. The mass spectra were calibrated externally using the exact masses of sodium formate clusters. The spectra were evaluated using DataAnalysis 4.4 software from Bruker. The samples were analyzed in water at 0.1 mM total ligand concentration and 1:1, 1:2 and 1:3 metal to ligand ratio. The sample solutions were introduced into the ESI source with a syringe pump (ColeParmers Ins. Co., Vernon Hills, IL, USA) at a flow rate of 3 μL min^{-1}.

2.6. EPR spectroscopy and deconvolution of the spectra

X-band CW-EPR spectra were recorded with a BRUKER ELEXSYS E500 spectrometer (microwave frequency 9.4 GHz, microwave power 13 mW, modulation amplitude 5 G, modulation frequency 100 kHz). In these experiments, the samples contain 3 mM phenanthroline-mono-*N*-oxide (or its derivatives) and the copper(II) to ligand ratios were varied between 1:1 and 1:3. Room temperature EPR spectra have been recorded in capillaries using 8 scans. Before simulating the spectra, all experimental spectra were corrected with the background spectrum of pure aqueous solution. Frozen solution EPR spectra were measured in quartz EPR tubes placed into Dewar containing liquid nitrogen at 77 K. 0.2 mL aliquots of samples were placed into the tubes and 0.05 mL MeOH was added as a cryoprotectant to prevent aggregation and crystallization of water upon freezing.

All measured CW-EPR spectra were simulated individually using a designated EPR software [14], moreover, the room temperature EPR spectra of the copper(II)-phenO system were simulated simultaneously by the „two-dimensional" method using the designated 2D_EPR program. In these calculations, the component EPR spectra and the formation constants are fitted simultaneously on the basis of mass-balance equations as it was reported elsewhere [15]. For the decomposition of room temperature EPR spectra, each component curve was described by the isotropic EPR parameters g_o, A_o^{Cu} copper hyperfine and a_o^N nitrogen hyperfine couplings, and the relaxation parameters α, β, γ which define the linewidths in the equation $\sigma_{MI} = \alpha + \beta M_I + \gamma M_I^2$, where M_I denotes the magnetic quantum number of copper nucleus. The anisotropic spectra were analysed by taking into account the anisotropic (rhombic or axial) EPR parameters (g_x, g_y, g_z, A_x^{Cu}, A_y^{Cu}, A_z^{Cu}, a_x^N, a_y^N, a_z^N, and the orientation dependent linewidth parameters) of the components. Since a natural $CuCl_2$ was used for the measurements, the spectra were calculated as the sum of the spectra of ^{63}Cu and ^{65}Cu weighted by their natural abundances. The copper and nitrogen coupling constants and the relaxation parameters were obtained in field units (Gauss = 10^{-4} T) and converted to wavenumber unit (cm^{-1}).

The EPR spectrum of the dimeric complex was simulated by the DNP module of the "EPR" program developed for calculating EPR spectra and dynamic nuclear polarization in coupled-spin systems (biradicals and paramagnetic dimers).[14,16] The EPR spectrum is calculated by the complete diagonalization of the Hamiltonian of a two-spin system. The principal values and orientation of $\mathbf{g_1}/\mathbf{g_2}$- and $\mathbf{A_1}/\mathbf{A_2}$-tensors were treated identically and the dipolar interaction (D), and exchange interaction (J) between two spin centres were calculated. Their relative orientation were characterized by the three Euler angles (α, β, and γ) and the relative position of the two centres is further described by two polar angles (χ, ψ), which defines the position of the connector line between the copper(II) centres in the frame of $\mathbf{g_1}$.

2.7. X-ray diffraction crystallography

Aqueous methanolic solution of $NiCl_2$ or $CuCl_2$ was mixed with the corresponding *N*-oxide (phenO or DMPO) and these solutions were stirred for 2 h at room temperature. Then NaOH was added to initiate complex formation processes and adjust the pH of the samples to slightly alkaline. These solutions were kept in refrigerator to allow the solvent to evaporate slowly. After some period of time, crystals suitable for diffraction measurements were harvested. Diffraction data of $[Ni(phenO)_2(CO_3)] \times 2H_2O$ were measured on a Bruker V8 Venture SCXRD system with Mo-Kα radiation (λ = 0.71074 Å) at room temperature. The data set $[Cu(DMPO)_2Cl]Cl \times CH_3OH$ were collected on a Rigaku RAXIS-RAPID II diffractometer using Mo-*K* α radiation at room temperature.

The data processing was managed by WinGX [17] or Olex^2 [18] programs including SIR [19] and SHELX [20] programs. Structures were validated with PLATON [21] and the publication materials were prepared by the Olex^2 and Mercury CSD-4.3.0 software.[22] CCDC-2204961 for $[Cu(DMPO)_2Cl]Cl \times CH_3OH$ and CCDC-2205576 for $[Ni(phenO)_2(CO_3)] \times 2H_2O$ contain the supplementary crystallographic data for this paper. These data can be obtained free of charge from The Cambridge Crystallo-graphic Data Centre via https://www.ccdc.cam.ac.uk/data_request/cif.

2.8. Computational details

Optimizations of the complexes formed between copper(II) and phenO-s were computed with the ORCA package [23] using the hybrid Becke three-parameter B3LYP functional [24,25] coupled with the Grimme's D3 dispersion.[26] The triply polarized "core properties" (CP(PPP)) basis set [27] was used for copper(II), the Barone "EPR-II" basis set [28] for nitrogen and the split-valence Pople basis set 6-311g(d,p) for the main group elements. Tight SCF convergence criteria were used in the geometry calculations. Single-point frequency calculations were carried out with the same functional and basis sets for the ground state geometries which represented true minima on the potential energy surface (No imaginary frequencies were found). In all cases, PCM model was used to take into account the effect of solvent (water).[29] Finally, single-point calculation for the optimized geometries was carried out to predict the EPR parameters of the copper(II) complexes.

3. Results and discussion

3.1. Protonation equilibria and spectrofluorometric features of the ligands

The acid dissociation constants of phenO and its derivatives obtained by pH-potentiometry are in excellent agreement with previously determined data.[10] Now, we focus on the fluorescence of these ligands. Since the phenanthroline backbone exhibits characteristic strongly pH dependent emission properties, the same scenario is expected for the *N*-oxides.

As an example, Fig. 1 shows the steady-state fluorescent emission spectra of phenO as a function of pH. At 280 nm exciting light, the spectra exhibit intense emission bands at 461 nm under acidic conditions and at 395 nm in basic solution. In accordance with previous literature, these bands are assigned to the lowest π-π* level.[30] The lifetime of the excited state is short and falls into 4–8 ns range estimated by laser flash photolysis (Table 1). The emission intensities were used to estimate the acid dissociation constants of all phenO-s. In diluted sample of phenO-s, the fluorescence intensity is directly proportional to the concentration, thus the emission data between 320 and 600 nm were fitted simultaneously to equation (1).

$$I = \frac{a_{HL}[H^+] + a_L K_a}{[H^+] + K_a} c_{tot} A_0 \Phi_f \quad (1)$$

where I is the fluorescent intensity at a given wavelength (λ), α_{HL} and α_L

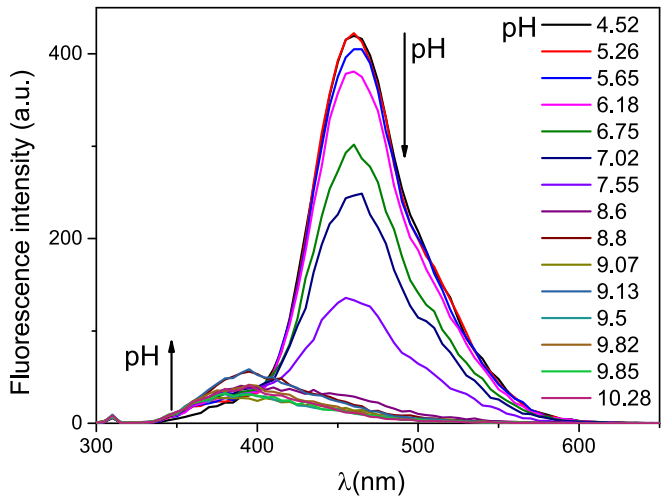

Fig. 1. Steady-state fluorescent spectra of phenO as a function of pH. Excitation wavelength: 280 nm, c_{phenO} = 20 μM.

Table 1
Acid dissociation constants, fluorescence emission maxima and fluorescence lifetimes of phenO, DMPO and TMPO at 25 °C (I = 0.2 M KCl).

	pK_a [a]	pK_a [b]	λ_{ex} (nm)	λ^c_{em} (nm)	λ^d_{em} (nm)	τ (ns)[c, e]	τ (ns)[d, e]
phenO	6.86 ± 0.03	6.86 ± 0.01	280	461	395	4.5 ± 0.2	7.6 ± 0.1
DMPO	8.44 ± 0.02	8.46 ± 0.01	290	462	[f]	4.7 ± 0.1	
TMPO	8.43 ± 0.02	8.42 ± 0.01	280	466	447	5.0 ± 0.1	6.4 ± 0.1

[a] Obtained by pH-potentiometry. [b] Calculated from steady-state fluorescent spectra recorded by Jasco FP-8500 spectrofluorometer. [c] Recorded in 0.1 M HCl. [d] Recorded in 0.1 M NaOH. [e] Fluorescence lifetimes were estimated by laser flash photolysis. [f] Disappeared in 0.1 M NaOH.

are the molar extinction coefficients for the protonated and deprotonated forms at λ, K_a is the acid dissociation constant and c_{tot} is the analytical concentration of phenO, A_0 is a machine constant and Φ_f is the fluorescence quantum yield.

Table 1 summarizes the pK_a-s and the fluorescence lifetimes obtained by laser flash photolysis. Although the ligands were used at μM concentration level in the fluorescent experiments, the results are in excellent agreement with those obtained by pH-potentiometry earlier at considerably higher ligand concentrations. [10].

In general, the formation of N—O bond increases the basicity of the ligands compared to the corresponding phens. The presence of the electron donating methyl substituents is associated with significant increase in the basicity of the ligand, i. e., the pK_a-s of DMPO and TMPO are higher by about 1.5 than that of phenO. Interestingly, the introduction of two or four methyl groups leads to the same change in the basicity. There is no straightforward explanation for this observation. Perhaps, the methyl substituents of TMPO are located far from the protonation site and have weaker effect on the basicity than expected.

3.2. Complex formation processes between phenO and copper(II) or nickel(II)

The complex formation reaction between copper(II) and phenO was studied by pH-potentiometric, EPR and UV–vis spectroscopic methods. The stability constants were evaluated by simultaneously fitting pH-potentiometric and EPR spectroscopic data, and the results are reported in Table 2. The equilibrium model was corroborated by pH-dependent relaxivity measurements as discussed in subsequent part of the paper (Fig. S1). The distribution curves of the complexes in the Cu(II)-phenO 1:2 system are shown in Fig. 2.

Table 2
Overall stability constants (log β_{pqr}, upper part of the table) and stepwise stability constants (log K) of Cu(II) and Ni(II) complexes formed with phenO-s.

	phenO		**DMPO**	**TMPO**	**phen** [a]	
	Cu(II)	Ni(II)	Cu(II)	Ni(II)	Cu (II)	Ni(II)
ML	6.28 ± 0.04[b] 6.61 ± 0.02[c]	5.0 ± 0.1	6.80 ± 0.01	5.56 ± 0.04	9.20	8.65
ML(OH)				–2.81 ± 0.04	2.07	
$ML(OH)_2$				–12.91 ± 0.02	–5.21	
ML_2	12.98 ± 0.06[b] 13.13 ± 0.02[c]	9.9 ± 0.1	12.00 ± 0.02	11.92 ± 0.02	15.90	16.70
$ML_2(OH)$[d]	1.98 ± 0.08		5.87 ± 0.03			
$M_2L_4(OH)_2$	7.8 ± 0.3[b] 8.4 ± 0.1[c]					
$logK_1^{ML}$	6.28 ± 0.04[b] 6.61 ± 0.02[c]	5.0 ± 0.1	6.80 ± 0.01	5.56 ± 0.04	9.20	8.65
$logK_{ML}^{ML(OH)}$				8.37 ± 0.04	7.13	
$logK_{ML(OH)}^{ML(OH)_2}$				10.10 ± 0.04	7.28	
$logK_2^{ML_2}$	6.70 ± 0.06[b] 6.52 ± 0.02[c]	4.9 ± 0.1	5.20 ± 0.02	6.36 ± 0.04	6.70	8.05
$logK_{ML_2}^{ML_2(OH)}$	11.15 ± 0.08		6.13 ± 0.03			
$logK_1/K_2$ [e]	–0.42	0.1	1.60	–0.80	2.50	0.60

[a] Data are taken from ref. [31–33] [b] Calculated from pH-potentiometry. [c] Calculated from EPR spectroscopy. [d] Calculated from EPR spectroscopy and kept fixed during the final fitting process of pH-potentiometric data. [e] $\log K_1/K_2 = 2\log\beta_{ML} - \log\beta_{ML2}$.

In the case of the Cu(II) – phenO system, the experimental results can be fitted well by considering the formation of $[Cu(phenO)]^{2+}$, $[Cu(phenO)_2]^{2+}$, $[Cu(phenO)_2(OH)]^{+}$ and $[Cu_2(phenO)_4(OH)_2]^{2+}$ complexes. The formation of a precipitate above pH 5 prevented the use of the alkaline region of the titration curves when the reactants were applied in equimolar concentration ratio. However, the titration curves were fitted in the entire pH-range at the metal to ligand ratios between 1:2 and 1:3.

The complex formation reaction starts in acidic pH range with the $[Cu(phenO)]^{2+}$ complex, however, the formation of the bis complex,

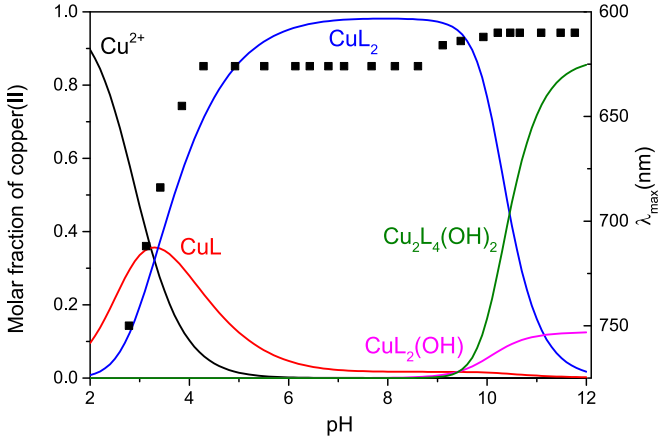

Fig. 2. The concentration distribution of the complexes formed between copper (II) and phenO and the λ_{max} values (■) as a function of pH at 1:2 metal to ligand ratio (I = 0.2 M (KCl), T = 298 K). c_{phenO} = 3 mM.

$[Cu(phenO)_2]^{2+}$, overlaps with this process. This is due to the unique feature of this system that the stepwise stability constants for the formation of the mono and bis complexes are practically the same (Table 2). Information on the coordination mode of $[Cu(phenO)]^{2+}$ was extracted from pH dependent EPR spectra. In acidic samples, the EPR spectra can be fitted well by considering the formation of a complex beside the free copper(II) ion. The complex exhibits $g_z = 2.330$ and $A_z = 157.7 \bullet 10^{-4}$ cm^{-1} spin Hamiltonian parameters (Table 3) which slightly differ from those obtained for the $[Cu(bpy)]^{2+}$ (bpy = bipyridine) complex ($g_z = 2.307$ and $A_z = 170 \bullet 10^{-4}$ cm^{-1}).[34] As expected, this leads to the conclusion that copper(II) is bounded to a nitrogen donor of phenO and to an oxygen atom in the equatorial plane yielding a 6-membered chelate structure in this complex. This complex is about 3 orders of magnitude less stable than the corresponding $[Cu(phen)]^{2+}$ [33] confirming that phenO is suitable to accommodate copper(II), but the formation of a larger chelate ring is less favorable. Upon increasing the pH, the formation of $[Cu(phenO)_2]^{2+}$ is associated with significant changes in the UV–vis (Fig. S2) and EPR spectra (Fig. 3 and S3, S4) as well as in relaxivity (Fig. S1). As shown in Fig. S2, the ca. 140 nm blue shift in the absorption maxima strictly correlates with the formation of the bis complex.

Table 3
Anisotropic and isotropic spin-Hamiltonian parameters determined by the simulation of the room temperature and frozen solution EPR spectra recorded for the Cu(II)-phenO, DMPO and TMPO systems in 80% H_2O/MeOH solvent mixture.

Complex	Isotropic parameters [a]			Anisotropic parameters [a]			
	g_0	A_0 / $\bullet 10^{-4}$ cm^{-1}	a_0^{N1} / a_0^{N2} / $\bullet 10^{-4}$ cm^{-1}	g_x, g_y, g_z	A_x,A_y, A_z / $\bullet 10^{-4}$ cm^{-1}	a_x^{N1} a_y^{N1}, a_z^{N1} / a_x^{N2} a_y^{N2}, a_z^{N2} / $\bullet 10^{-4}$ cm^{-1}	$g_{0,calc.}$ [b]
phenO							
Cu_{aq}^{2+}	2.195	31.2		2.080, 2.080, 2.415	11.3, 11.3 131.1		2.192
[CuL]	2.156	51.5	13.6	2.060, 2.060, 2.330	5.7, 5.7, 157.7	9.6, 9.6, 8.7	2.150
$[CuL_2]$	2.129	64.1	11.3 11.3	2.044, 2.061, 2.275	19.4, 2.8, 170.2	5.7, 13.3, 10.4 11.1, 12.9, 9.1	2.127
$[CuL_2(OH)]$	2.120	75.2	6.9 6.9	2.045, 2.057, 2.263	22.5, 19.9, 180.7	9.6, 5.8, 6.3 9.8, 13.5, 6.3	2.121
DMPO							
[CuL]	2.160	50.0	13.6				
$[CuL_2]$	2.128	62.6	12.7 12.7	2.029, 2.078, 2.263	25.2, 40.6, 156.8	11.6, 6.0, 6.0 9.6, 6.0, 6.0	2.124
TMPO							
[CuL]				2.054, 2.054, 2.330	9.6, 9.6, 157.7	15.3, 11.6, 7.4	2.146
$[CuL_2]$				2.048, 2.065, 2.265	23.9, 13.3, 175.7	15.3, 11.6, 7.4 15.3, 11.6, 7.4	2.126
dimer [c]				2.055, 2.055, 2.260	24.0, 24.0, 175.0		2.123

[a] The experimental error were ± 0.001 for g_0, ± 0.3•10^{-4} cm^{-1} for A_0, ±0.002 for g_x and g_y, ±0.001 for g_z, ± 2•10^{-4} cm^{-1} for A_x and A_y and ± 1•10^{-4} cm^{-1} for A_z. [b] Calculated by the equation $g_{0,calc} = (g_x + g_y + g_z)/3$. [c] Euler angles (α,β,γ) are 0.0° and Polar angles $\chi = 15°$ and $\psi = 0.0°$, D = 393 G, J > 1500 G, Cu-Cu distance 3.78 Å.

According to simple statistical considerations, the coordination of the second ligand is less probable compared to the first one and $\log K_1$ should be higher than $\log K_2$ by 0.6 in the absence of special effects. Typically, steric, geometric, and electrostatic effects result in considerably larger differences between these equilibrium constants in many systems. In our case, $\log K_1$ and $\log K_2$ are about the same (Table 2) and it leads to the conclusion that the formation of the bis complex is favorable. The similar values of the stepwise stability constants also strongly suggest that the two phenO-s coordinate to copper(II) in the same manner which can be envisioned by considering either elongated octahedral, square-pyramidal or trigonal bipyramidal coordination environments. In order to gain further insight into the structure of the bis complex in solution, relaxometric measurements were carried out (Fig. S1). Earlier studies confirmed that the paramagnetic contribution to the relaxation rate of water protons differs in the equatorial and axial positions of the coordination sphere of copper(II). This is due to the Jahn-Teller distortion, i.e. the axially coordinated water molecules are not capable to transfer the paramagnetic relaxation effect of the metal center into the relaxation of the bulk water because of the elongated apical Cu(II)-O_{wat} distance. On the basis of the equilibrium model, the relaxivity of each copper(II) complex was calculated by solving the overdetermined linear equation system. This calculation yields $r_{2p} = (3.4 \pm 0.4) \bullet 10^2$ $M^{-1}s^{-1}$ for the $[Cu(phenO)_2]^{2+}$ complex which is in reasonable agreement with the relaxivity reported for the $[Cu(bpy)_2]^{2+}$ complex featuring an equatorially coordinated water molecule, $r_{2p} = 6.8 \bullet 10^2$ $M^{-1}s^{-1}$. [35] This strongly suggests that one of the water molecules is relatively close to the copper(II) center in $[Cu(phenO)_2]^{2+}$, consequently, the elongated octahedral geometry can be ruled out.

For the $[Cu(bpy)_2(H_2O)_2]^{2+}$ complex, Noack and Gordon proposed the formation of *cis* and *trans* isomers in EtOH-H_2O solvent mixture [36], while Garribba et al. detected only one species in aqueous solution with inverse EPR parameters ($g_{x,y} > g_z$).[34] In a solution containing Cu(II) and phenO in 1:2 ratio, the EPR revealed the formation of an exclusive species with $g_z = 2.275$ and $A_z = 170.2 \bullet 10^{-4}$ cm^{-1} spin Hamiltonian parameters. These EPR parameters of the bis complex unambiguously confirm the presence of a $d_{x^2-y^2}$ ground state of copper(II) in an elongated octahedral or square-pyramidal coordination environment. Since

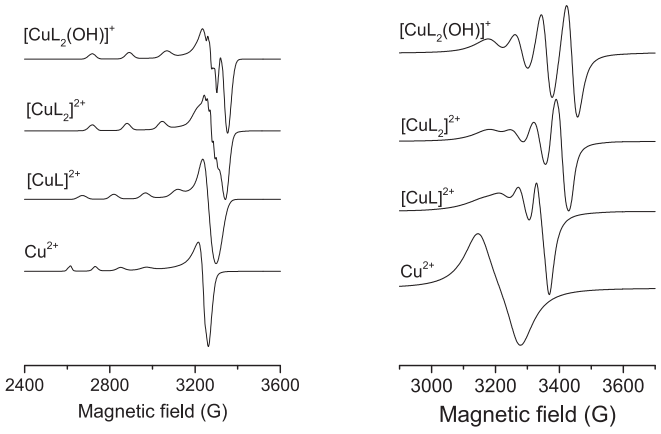

Fig. 3. Calculated component EPR spectra obtained for the copper(II)-phenO complexes on the basis of the evaluation of the pH-dependent frozen solution (left) and room temperature (right) EPR spectra. The EPR spectra of the dimeric species are not shown.

the spin Hamiltonian parameters are not compatible with the trigonal bipyramid sphere and the octahedral geometry is ruled out on the basis of relaxivity measurements, the bis complex must possess a square-pyramidal coordination environment with $[Cu(H_2O)(phenO)_2]$ stoichiometry. In this complex, the phenO-s coordinate at the corners of the square and the remaining site is occupied by the water molecule.

The formation of the bis complex with phenO was also confirmed by HR-MS measurements; the experimental and calculated *m/z* values, as well as the isotope pattern, are in good agreement with the proposed complex (Fig. S5).

The hydrolysis of the coordinated water molecule yields a mixed hydroxo species, $[Cu(phenO)_2(OH)]^+$, in alkaline solution. Slight changes in the absorption spectra confirms this process, moreover, the relaxivity increases drastically which is due to the enhanced relaxation effect via the proton exchange of the coordinated hydroxide ion.[35] Interestingly, significant decrease in the EPR intensity was observed both in frozen solution and room temperature spectra by increasing the pH. This is unambiguously due to the formation of 'EPR silent' dimeric species most likely with $[Cu_2(phenO)_4(OH)_2]^{2+}$ stoichiometry. Such species can readily be envisioned, when the two copper(II) centers are linked through μ-OH bridges. The formation of a similar μ –OH bridged copper(II) complex, $[Cu(bpy)(OH)]_2^{2+}$, was reported in the Cu(II)-bpy system.[37] Since the proton consumption per metal ion is the same for the formation of $[Cu(phenO)_2(OH)]^+$ and $[Cu_2(phenO)_4(OH)_2]^{2+}$ complexes, pH-potentiometry is not suitable to distinguish the monomeric and dimeric species. Room temperature EPR spectra were used to estimate the overall stability constant of these species and to refine the equilibrium model. The equilibrium constant of the dimerization, K_D, is expressed as follows.

$$\log K_D = \log \beta[Cu_2(phenO)_4(OH)_2] - 2 \times \log \beta[Cu(phenO)_2(OH)] \quad (2)$$

The estimated value of log K_D is 4.4 indicating that the formation of the dimeric species is highly preferred over the monomer. Fig. 4 shows the calculated structures of the monomeric and dimeric species by the DFT method and the corresponding Cartesian coordinates are collected in Table S1 and S2. For the mononuclear complex, the calculated A_z value ($163.9 \bullet 10^{-4}$ cm^{-1}) is in reasonable agreement with the experimental value ($A_z = 180.7 \bullet 10^{-4}$ cm^{-1}) confirming the structure of the complex in solution. In this complex, one of the phenO-s binds *via* the (N, O) donors in the equatorial plane of copper(II). The next phenO occupies the equatorial plane by the aromatic N and the axial position by O donor atoms, while hydroxide ion binds in the remaining position of the equatorial plane (Fig. 4) yielding a square-pyramidal coordination environment.

In the dimeric complex, the hydroxide ions act as bridging ligands between the metal centers which feature distorted octahedral coordination geometry each binding two phenO-s. It is important to note, that the dimeric species formed in the Cu(II)-bpy system with $[Cu_2(bpy)_4(OH)]^{3+}$ stoichiometry contains an exclusive hydroxide bridge.[35] Incorporation of $[Cu_2(phenO)_4(OH)]^{3+}$ complex in the equilibrium model is not suitable for the interpretation of the pH-potentiometric and EPR data. The noted difference between the two systems can be explained by considering the different ring size of the chelates formed with bpy and phenO, moreover, the geometry around the copper(II) centers differs in the two systems. In the $[Cu_2(bpy)_4(OH)]^{3+}$ complex, the 5-membered chelate of bpy provides rigid and compressed coordination environment which hinders the binding of another hydroxide ion. In contrast, the dimeric species formed in the Cu(II)-phenO system has a larger 6 membered chelate structure and due to the presence of N—O bond, phenO rotates out from the equatorial plane of copper. This provides a readily accessible coordination sites for both hydroxide ions leading to the formation of the $[Cu_2(phenO)_4(OH)_2]^{2+}$ complex. The distance between the Cu(II) centers obtained from the DFT optimized structure is relatively short, d = 2.96 Å, and the DFT calculations predict a spin exchange coupling of –78.8 cm^{-1}. This is consistent with the lack of an EPR signal, i. e., a typical doublet pattern cannot be observed in the EPR spectrum due to the antiferromagnetic coupling between the Cu(II) centers. For the crystal structure of the $[Cu_2(\mu\text{–}OH)_2(bpy)_2(SO_4)(H_2O)] \times 4H_2O$ complex, the same kind of OH-bridged structure was reported with 2.89 Å distance between the Cu(II) centers [37] which is in reasonable agreement with the calculated distance in the copper(II)-phenO system (d = 2.96 Å).

Earlier the formation of stable tris complexes were reported in the Cu(II)-bpy and Cu(II)-phen systems.[38] The formation of such a complex can be ruled out on the basis of equilibrium and spectroscopic studies in the Cu(II)-phenO system. This is due to the differences of the chelate ring size again. The bpy and phen ligands form compact 5-membered chelate rings and coordinate in *cis* position in the corresponding octahedral bis complexes. This geometry makes possible the relatively strong coordination of the third ligand. The considerably larger 6-membered chelate rings formed with phenO sterically hinder the coordination of the third

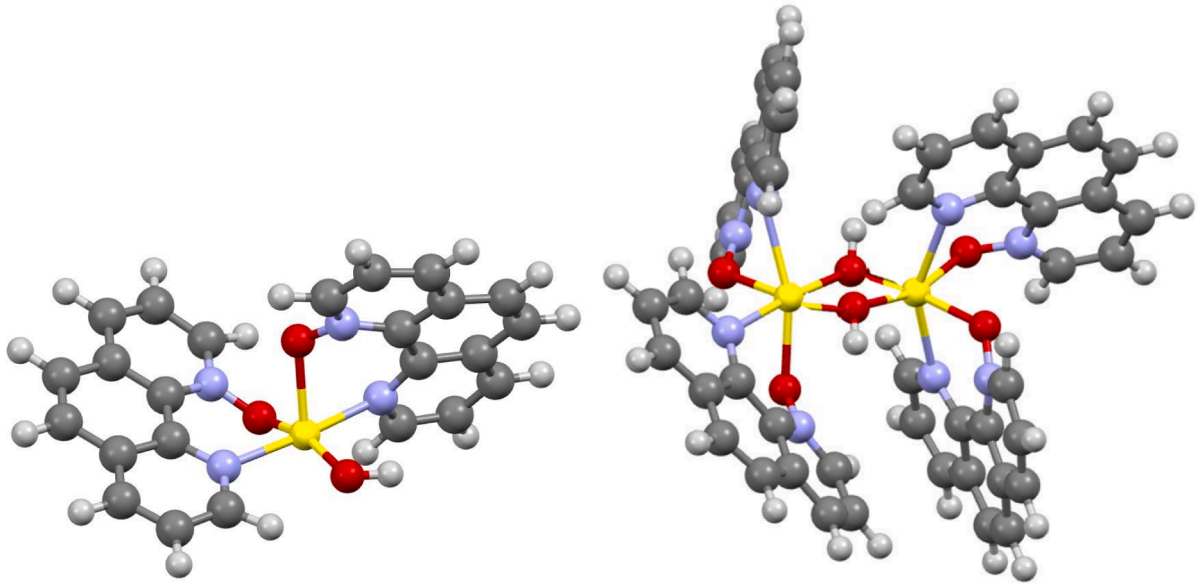

Fig. 4. DFT optimized structures of the $[CuL_2(OH)]^+$ and $[Cu_2L_4(OH)_2]^{2+}$ complexes formed in the Cu(II)-phenO system.

chelate.

The complex formation processes between Ni(II) and phenO show distinct features compared to the Cu(II)-phenO system. While precipitation was observed above pH 8.0 at 1:1 metal ion to ligand concentration ratio, no evidence was found for the formation of ternary hydroxo complexes at ligand excess. The corresponding distribution curves of the complexes in the Ni(II)-phenO system are shown at 1:2 metal to ligand ratio in Fig. S6. pH dependent UV–vis spectra demonstrate that the formation of the $[Ni(phenO)_2]^{2+}$ complex is associated with a characteristic spectral change in the 420 – 600 nm region (Fig. S7) confirming square-planar geometry and the diamagnetic feature for this species. The mono- and bis complexes are considerably less stable than the corresponding complexes formed with phen (Table 2) indicating that accommodation of the six-membered chelate rings in the coordination sphere of Ni(II) is less favorable compared to the five-membered rings. In HR-MS experiments, the agreement between the experimental and calculated *m/z* values as well as the isotope patterns unambiguously confirmed the exclusive existence of the bis complex (Fig. S8). Slow evaporation of methanolic solution of Ni(II)-phenO samples yielded red crystals suitable for X-ray analysis. These measurements revealed that two phenO ligands and a CO_3^{2-} anion are attached to the nickel(II) ion (Fig. 5, Fig. S9, Table S3) and two water molecules are latticed to the neutral complex. The CO_3^{2-} anion is required to maintain the overall neutral charge of the molecule. (The source of carbonate ion is adventurous CO_2 trapped in the slightly alkaline solution from air.).

X-Ray studies on the $[Ni(CO_3)(Phen)_2] \times 2H_2O$ complex are available in the literature,[39] however, to the best of our knowledge, $[Ni(phenO)_2(CO_3)] \times 2H_2O$ is the first molecular structure of a Ni(II)-phenO complex in the CSD. The asymmetry unit contains half of the complex which crystallizes in the orthorhombic crystal system in non-centrosymmetric *Fdd*2 space group (Fig. S10). The other part of the complex was generated by (*-x*, *-y*, *z*) symmetry operation and the Ni(II) ion exhibits a distorted octahedral geometry similar to $[Ni(CO_3)(Phen)_2]$. Consequently, the square-planar structure formed in aqueous solution is altered to maintain the neutral charge of the crystal in solid state. Nickel(II) binds to two oxygen (2.009(8) Å) and two nitrogen atoms (2.027(10) Å) and two oxygen atoms of carbonate anion (2.060 (9) Å) (Fig. S11). For the carbonate group, the O2-Ni-$O2^i$ bond angle is 64.94° and the two O2-C1 lengths are significantly longer (coordinated O atom, 1.300(11) Å) than the O3-C1 distance (1.250(5) Å) confirming the bidentate coordination of the anion.

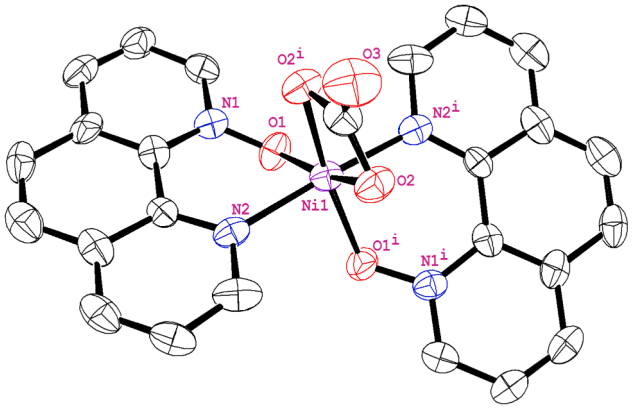

Fig. 5. ORTEP representation of the crystal structure of $[Ni(phenO)_2(CO_3)]$ shown with 50% probability level. Water molecules and hydrogens are omitted for clarity. Symmetry code: (*-x*,*-y*, *z*). Selected bond distances(Å) Ni1–O2 = 2.060(9), Ni1–$O2^i$ = 2.060(9), Ni1–$O1^i$ = 2.009(8), Ni1–O1 = 2.009(8), Ni1–N2 = 2.027(10), Ni1–$N2^i$ = 2.027(10), O2–C1 = 1.300(11), O3–C1 = 1.25 (2), O1–N1 = 1.334(14). Further bond lengths and angles are available in the SI, Table S4 and S5.

Furthermore, the phenanthroline skeletons in the crystal are twisted, with the donor atoms N2 and O1 displaced farthest from the best-plane (N1, C13, C5, C4, C2, C3) of the phenanthroline *N*-oxide group by 0.414 and −0.256 Å (Fig. S12). Almost the same distortions were observed in the crystal of $[PtBrMe_2(CH_2C_6H_4\text{-}4\text{-}t\text{-}Bu)(phenO)]$ [40] (0.4 and −0.29 Å) and somewhat smaller ones for $[CuCl_2(phenO)_2]$[41] (0.23 and −0.25 Å). Packing arrangement of the complexes viewed from the three crystallographic directions are shown in Fig S13. Despite the presence of phenO rings, only very weak π –π interactions formed but strong hydrogen bonds exist between water molecules(O4) and O3 [O4-H4…O3 = 2.751 Å (Fig. S14 and Table S6).

3.3. Complex formation processes of DMPO and TMPO

DMPO and TMPO exhibit certain selectivity in the complex formation reactions with Cu(II) and Ni(II). While DMPO forms relatively stable complexes with copper(II), the coordination of this ligand to nickel(II) could not be confirmed under the experimental conditions applied in this study. Mixing copper(II) with TMPO in various concentration ratios leads to the formation of precipitate with unknown composition in the entire studied pH range (pH 2.0 – 11.0). In contrast, TMPO forms stable water soluble nickel(II) complexes. These observations can be explained by considering the well-known differences in the coordination chemical features of the two metal ions. Copper(II) is usually characterized by non-rigid coordination geometries that is often termed as the plasticity of copper(II) (compressed and octahedral structures, tetra- and penta-coordinated species etc.), [42] while the diamagnetic nickel(II) complexes possess rigid, square-planar coordination geometry. The methyl substituents are located in 2 and 9 positions in DMPO, and most likely they sterically hinder the distortion of the planar *N*-heteroaromatic rings required for occupying the square planar coordination sites of Ni(II). In the case of Cu(II), this ligand with the bulky substituents near to the donor atoms can be accommodated in a distorted *cis*-octahedral or a distorted square pyramidal structure. In other words, the plasticity of copper(II) allows the distortion of the geometry, and DMPO may twist out from the equatorial plane to minimize steric hinderances. This is confirmed by the X-ray structure of the complex detailed in subsequent part of the paper. This plasticity may also be a key factor in the copper (II) – TMPO system assuming that the distortion of the geometry favors hydrophobic interactions and the hydrophobic moieties of the ligand destroy the structured hydration sphere around the complex. As a consequence, the solubility of the complex decreases and precipitation forms. In TMPO, the methyl substituents are relatively far from the donor atoms, and the ligand can easily occupy the rigid square-planar coordination sites around nickel(II). This tight structure prevents intermolecular hydrophobic interactions and the complexes remain soluble in water.

The complex formation process between Cu(II) and DMPO starts in the acidic pH range with the formation of $[Cu(DMPO)]^{2+}$ complex. The stability of the $[Cu(DMPO)]^{2+}$ complex is ca. 1 order of magnitude higher than the stability of the $[Cu(phenO)]^{2+}$ complex which can readily be explained by considering the different basicities of the two ligands (Table 1). The absorption maximum at 710 nm is consistent with the binding of one DMPO, moreover, the room temperature EPR spectrum is similar to that of $[Cu(phenO)]^{2+}$ confirming the (N,O) binding mode in this complex. In contrast to the Cu(II)-phenO system, the mono complex $[Cu(DMPO)]^{2+}$ is the only major species in the pH range between 4 and 7 at room temperature (Fig. 6). In the EPR spectrum of the frozen solution, the component spectrum of $[Cu(DMPO)]^{2+}$ complex could not be distinguished from those of $[Cu(aqua)]^{2+}$ and $[Cu(DMPO)_2]^{2+}$.

Upon increasing the pH, a further DMPO binds to copper(II) leading to characteristic changes both in the UV–vis and EPR spectra (Figs. S15, S16 and Table 3). In comparison to the Cu(II)-phenO system, the formation of the bis complex is not preferred over the mono complex. Most likely, the methyl substituents in close vicinity to the donor atoms may

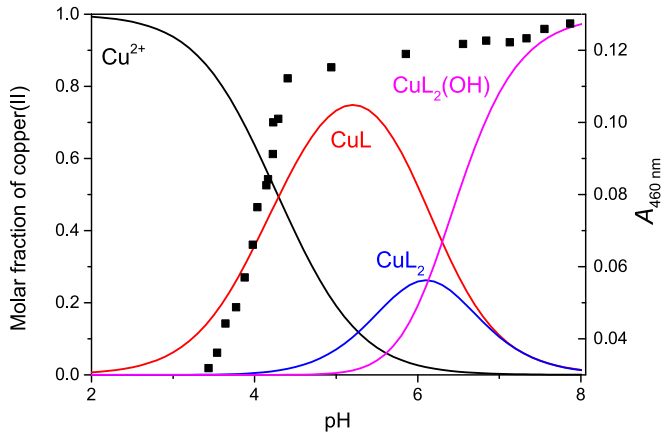

Fig. 6. The concentration distribution of the complexes formed in the copper (II) – DMPO system and the *A* values at 460 nm (■) as a function of pH at 1:2 metal to ligand ratio (I = 0.2 M (KCl), T = 298 K). c_{DMPO} = 3 mM.

hinder the binding of the second DMPO. The $\log K_1/K_2$ value (eq. 3), 1.60, corroborates this consideration.

$$\log K_1/K_2 = 2x\log\beta([Cu(DMPO)]) - \log\beta([Cu(DMPO)_2]) \quad (3)$$

Exclusively, the bis complex was observed under the experimental conditions of EPR spectroscopy at 77 K. The spectrum of $[Cu(DMPO)_2]^{2+}$ could be determined only below pH ~ 8 (Fig. S16) because the EPR signal disappeared in more alkaline solutions. This is most probably due to the formation of an EPR inactive dimeric hydroxo species. The isotropic parameter (g_0, A_0) values of complexes $[Cu(DMPO)_2]^{2+}$ and $[Cu(phenO)_2]^{2+}$ are very similar confirming the same coordination environment around the metal center. However, A_z is considerably smaller and the difference in g_x and g_y is about two times bigger for $[Cu(DMPO)_2]^{2+}$ than for $[Cu(phenO)_2]^{2+}$. This is consistent with the larger rhombic distortion of $[Cu(DMPO)_2]^{2+}$.

To characterize the structure of the bis complex in more detail, DFT calculations were performed. The calculated structure is shown in Fig. S17, and the corresponding Cartesian coordinates are reported in Table S7. First, an inner sphere water molecule was inserted into the coordination sphere of copper(II) and the effect of the surrounding water molecules was taken into account using the PCM model. DFT predicts a pentacoordinate copper(II) species where the oxygen atoms of the DMPO are in *trans* arrangement. It is important to note, that geometry optimization was also initiated from *cis* geometry, but the optimization steps yielded the *trans* arrangement. Due to the steric hinderance of the methyl substituents of DMPO, the two condensed aromatic rings of DMPO exhibit significant distortion, however, the coordinating donor groups are accommodated in the equatorial plane of copper(II). These results are consistent with those obtained by EPR spectroscopy. Moreover, the calculated g_0 (2.089) and A_z (179.6•10^{-4} cm^{-1}) values are in good agreement with the experimental values confirming the structure of the complex in solution.

Crystals of $[Cu(DMPO)_2Cl]Cl \times CH_3OH$ suitable for X-ray diffraction measurements were obtained from methanol by slow evaporation. Green, prism shaped crystals were harvested. The complex crystallized in the triclinic crystal system in *P*-1 space group. The asymmetric unit contains a bis complex with an axially coordinated chloride ion, one methanol molecule and one chloride as counter ion (Fig. S18). The unit cell, containing two molecules, and packing of the complexes viewed from the three crystallographic directions are shown in Figs. S19, S20. The coordination geometry around the copper ion is distorted square pyramidal with N and O donor atoms forming a plane and one chloride ion in apical position. The two nitrogen and the two oxygen atoms of DMPO are in *trans* positions (in agreement with the predicted structure in solution) and (Fig. 7). The distortion is characterized by the trigonality index of τ_5 = 0.75. [43].

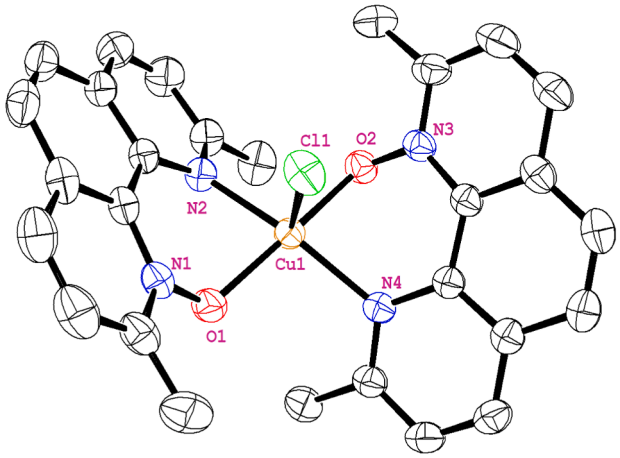

Fig. 7. ORTEP representation of the crystal structure of $[Cu(DMPO)_2Cl]^+$ shown with 50% probability ellipsoids. A chloride ion, hydrogens and methanol molecule are omitted for clarity. Selected bond distances (Å) and angles (°) are as follows: Cu1–Cl1 = 2.4900(6), Cu1–O1 = 1.9337(14), Cu1–O2 = 1.9233 (14), Cu1–N2 = 2.0446(17), Cu1–N4 = 2.0474(16), O1–N1 = 1.339(2), O2–N3 = 1.336(2). Further bond lengths and the bond angles are collected in the SI, Table S8 and S9.

Due to steric hindrance of methyl substituents, the two rings rotate out from the equatorial plane and the two phenanthroline rings are almost perpendicular to each other as it was also predicted by DFT. It is noteworthy that excellent agreement (bond lengths and angles) was found between the DFT calculated and the X-ray structures confirming the same structure and coordination mode both in solid state and solution phase (Fig. S17). The dihedral angle formed by the two ring planes is found to be 87.7° (Fig. S21). The plane of the first and second rings are at an angle of 46.46° and 41.77° to the equatorial plane, respectively. The length of the coordinated N—O bond is significantly longer than the N—O bond for the DMPO ligand (1.339 Å and 1.336 Å vs. 1.284 Å).[44] This is consistent with the results obtained for the $[Ni(phenO)_2(CO_3)]$ (1.334 Å for the complex and 1.320 for phenO [45]). When the N—O group is absent, the planar *N*-heteroaromatic ligands turn out from the equatorial plane as it was shown in the case of the *cis*-octahedral and trigonal bipyramidal crystal structures of $[Cu(phen)_2(H_2O)]_2NO_3$ [46] and $[Cu(bpy)_2(H_2O)]S_2O_6$,[47] respectively (Fig. S22).

Two complexes form a pair through a C—H …Cl bond, moreover a strong π …π off centred parallel stacking interaction exists between the two phenanthroline rings, where the distance between two ring centroids is 3.738 Å. Thus, the space between the columns formed by the ionic complexes is filled with methanol and chloride ion (Fig. S23, Table S10).

In the Cu(II)-TMPO system, precipitation was observed in the entire pH-range which is presumably due to the decreased solubility of the copper(II)-TMPO complexes. Nevertheless, EPR spectroscopy is suitable to investigate the complexes at 100 μM concentration level. Consequently, EPR was used to extract information on the coordination mode of the complexes formed in this system at 77 K and the structure of the complexes as a function of pH was studied using individual samples. In these experiments, different metal to ligand ratios were selected and the pH of the heterogenous system was adjusted by combined platinum ring electrode, then the precipitation was filtered, and the solution was introduced into the EPR tube. The EPR spectra as a function of pH are shown in Fig. S24 and the component EPR spectra obtained from the simulations are shown in Fig. 8.

The spectra (Fig. S24) can be fitted well by considering the $[Cu(TMPO)]^{2+}$, $[Cu(TMPO)_2]^{2+}$ and a dimeric species. In alkaline solution, the intensity of the EPR signal decreases significantly which is due to the formation of the diamagnetic copper(II) species. In slightly acidic pH

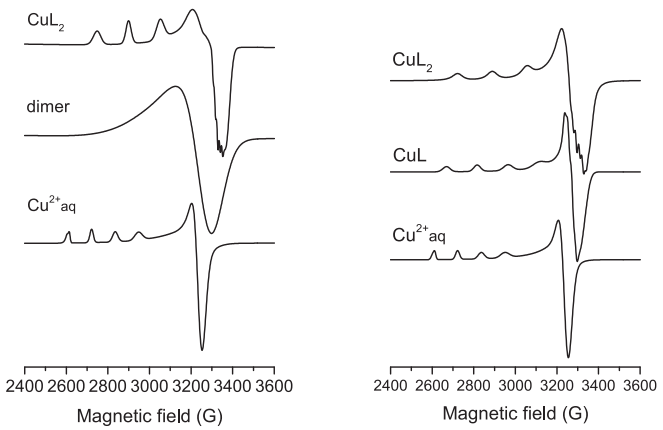

Fig. 8. Component EPR spectra obtained on the basis of the evaluation of the pH-dependent frozen solution EPR spectra in the Cu(II)-DMPO (left) and Cu(II)-TMPO (right) systems. The component spectrum of the dimeric species formed in the Cu(II)-TMPO system is not shown.

range, $[Cu(TMPO)]^{2+}$ complex forms. The corresponding anisotropic EPR parameters are the same that were found for $[Cu(phenO)]^{2+}$, thus copper(II) binds to TMPO via the (N,O) donor set. Upon increasing the pH, a further TMPO coordinates to the metal ion yielding the $[Cu(TMPO)_2]^{2+}$ bis complex. In this complex, the g_z and A_z values support that copper(II) is accommodated by two (N,O) donor sets. Beside the mono complexes, the formation of dimeric copper(II) complex was also observed in the EPR spectra. The well resolved doublet peak signal together with the half-field signal at 1600 G unambiguously prove the presence of coupled spin-system, thus, the presence of two copper(II) centers (Fig. 9).

Simulation of the spectrum yields the relative orientation of these centers, Polar angles $\chi = 15°$ and $\psi = 0.0°$, which indicates that one copper(II) center is above of the other. The dipolar coupling also provides the possibility to calculate the distance between the paramagnetic centers. This distance was estimated to be 3.78 Å. It deserves to be commented that very similar dimeric EPR spectrum was recorded for $[Cu(bpy)_2(OH)]_2^{2+}$ complex at high concentration (5×10^{-2} M) by Garribba et al. [34]. The distance between the copper(II) ion was estimated to be 3.4 Å for this complex. [34] In this case, copper(II) ions were suggested to possess compressed tetrahedral coordination geometry. As a further comparison, dimeric copper(II) complex of 8-hydroxyquinoline derivatives exhibits similar EPR spectra, (see Fig. S25), [48] where the

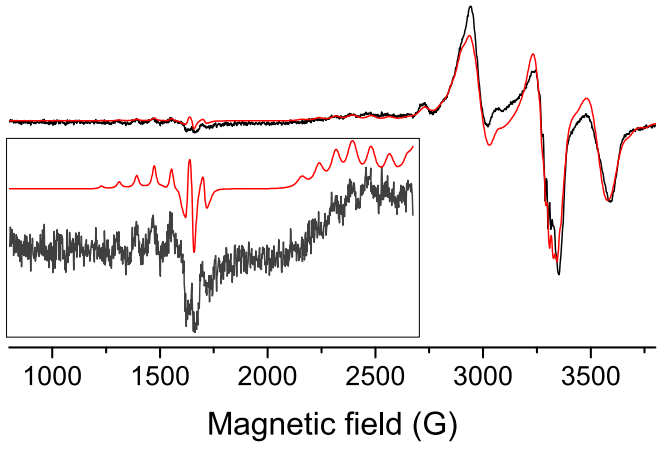

Fig. 9. Experimental (black) and simulated (red) frozen solution EPR spectra recorded for the Cu(II)– TMPO system in 80% H_2O/MeOH solvent mixture at pH 6.1 and at 77 K. The inset shows the 800–2700 G range of the spectrum. The spectrum was simulated by the sum of 9% CuL_2 and 91% dimeric species.

X-ray structure proved the equatorial-axial bridge coordination of ligand oxygen donor atom and the copper–copper distance of 3.39 Å was very close to the distance calculated by Garribba et al. [34] However, an OH-bridged dimeric structure cannot be ruled out, as was found in solid state for μ-hydroxo-tetrakis(bpy)dicopper(II) perchlorate complex in which the copper–copper distance was 3.645 Å (see Fig. S25). [49].

The equilibrium model of the nickel(II)-TMPO system can be fitted well by considering the formation of $[Ni(TMPO)]^{2+}$, $[Ni(TMPO)_2]^{2+}$, $[Ni(TMPO)(OH)]^{+}$ and $[Ni(TMPO)(OH)_2]$ species. The corresponding distribution curves of the complexes together with the absorbance values obtained at 480 nm are shown in Fig. 10.

The distribution curves clearly show that the $[Ni(TMPO)_2]^{2+}$ complex dominates in the entire pH range. The intensive absorption band at 480 nm confirms that this complex has a square-planar geometry and nickel(II) is bounded via the 2x(N,O) donor sets. The formation of this species was further corroborated by HR-MS spectroscopy, where the calculated m/z values and isotope patterns were in excellent agreement (Fig. S26). Upon increasing the pH, the binding of hydroxo group yields the formation of mixed hydroxo species, $[Ni(TMPO)(OH)]^{+}$ and $[Ni(TMPO)(OH)_2]$. Although one of the TMPO moieties is liberated by the hydroxo groups, these species also possess square-planar coordination environments which is confirmed by UV–vis spectroscopy. Any attempt to obtain crystals for X-Ray characterization was unsuccessful.

4. Conclusion

The results presented in this paper provide new insight into the coordination chemistry of phenanthroline-mono-*N*-oxides. The 1,10-phenanthroline-mono-*N*-oxide exhibits excellent metal binding ability, both copper(II) and nickel(II) form bis complexes which are dominant in whole pH range. The ligands bind to the metal ions via the (N,O) donor set and form 6-membered chelate rings. The bis complexes formed between copper(II) and 1,10-phenanthroline-mono-*N*-oxide possesses a coordinated water molecule near to the metal center providing a readily accessible coordination site. This feature may be utilized in systematic design of catalytic reactions.

Introduction of methyl substituents (DMPO and TMPO) yields selective metal binding ability in aqueous solution, as shown, copper(II) complexes form with DMPO and TMPO binds to nickel(II). In these complexes, the metal ions accommodate the (N,O) donor set. In the case of the bis complex formed between copper(II) and DMPO, significant distortion was observed. This is presumably due to the steric hinderance of the methyl substituents as it was confirmed by X-ray diffraction.

Finally, the results obtained for the copper(II) and nickel(II) complexes of phenanthroline-mono-*N*-oxide and its two derivatives provide solid background for exploring possible applications of these novel complexes in various fields of chemistry including homogeneous and heterogeneous catalytic redox reactions, altering electrodes for electrochemical purposes, preparing mild oxidants for synthetic chemistry etc.

Author contributions

The manuscript was written through contributions of all authors. All authors have given approval to the final version of the manuscript.

CRediT authorship contribution statement

Norbert Lihi: Writing – original draft, Writing – review & editing. **Nóra V. May:** Data curation, Writing – original draft. **Antal Udvardy:** Data curation, Writing – original draft. **Ferenc Najóczki:** Investigation. **Dóra Bonczidai-Kelemen:** Investigation. **Róbert Diószegi:** Investigation. **Dóra Szalóki:** Investigation. **Szófia O. Sánta:** Investigation. **István Fábián:** Writing – original draft, Writing – review & editing, Funding acquisition.

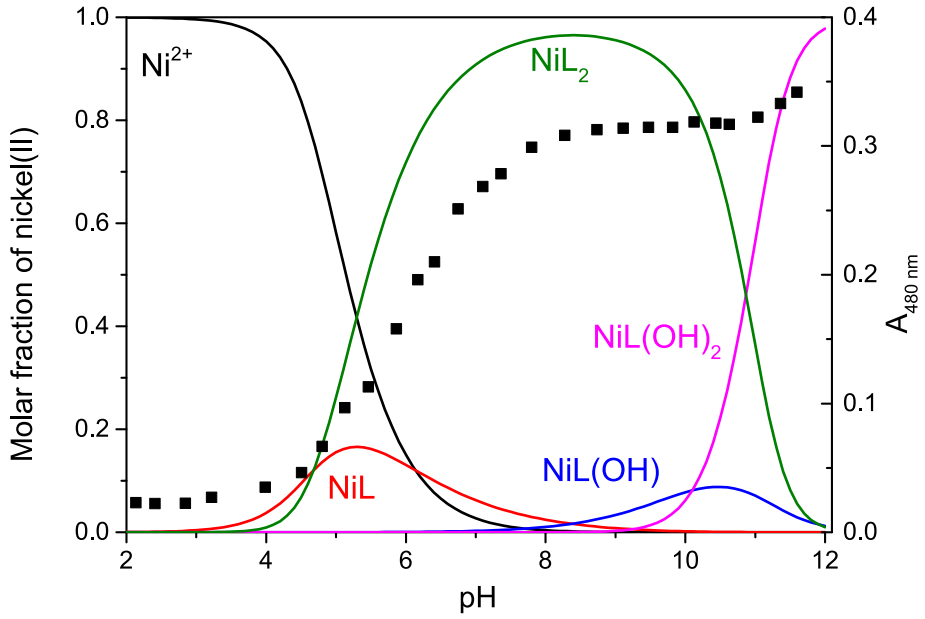

Fig. 10. Concentration distribution of the complexes formed between nickel (II)-TMPO and the *A* values at 480 nm (■) as a function of pH at 1:2 metal to ligand ratio (I = 0.2 M (KCl), T = 298 K). c_{TMPO} = 3 mM.

Declaration of Competing Interest

The authors declare that they have no known competing financial interests or personal relationships that could have appeared to influence the work reported in this paper.

Data availability

Data will be made available on request.

Acknowledgments

Support by the National Research, Development and Innovation Found (K-139140 and K-124544) is gratefully acknowledged. Project no. 1018348 has been implemented with the support provided by the Ministry of Culture and Innovation of Hungary from the National Research, Development and Innovation Fund, financed under the KDP-2020 funding scheme. N. L. acknowledges financial support of the János Bolyai Research Scholarship of the Hungarian Academy of Sciences. The authors are indebted to KIFÜ for awarding access to resource based in Hungary.

Appendix A. Supplementary data

Supplementary data to this article can be found online at https://doi.org/10.1016/j.ica.2023.121715.

References

[1] A. Bencini, V. Lippolis, Coord. Chem. Rev. 254 (2010) 2096–2180, https://doi.org/10.1016/j.ccr.2010.04.008.
[2] W. Yang, R. Zhang, F. Yi, M. Cai, J. Org. Chem. 82 (2017) 5204–5211, https://doi.org/10.1021/acs.joc.7b00386.
[3] R. Loska, Recent advances in cycloaddition reactions of heterocyclic N-oxides, in: O.V. Larionov (Ed.), Heterocyclic N-Oxides, Springer International Publishing, Cham, 2017, pp. 85–110, https://doi.org/.10.1007/7081_2017_2.
[4] P. Koukal, J. Ulč, D. Nečas, M. Kotora, Pyridine N-oxides and derivatives thereof in organocatalysis, in: O.V. Larionov (Ed.), Heterocyclic N-Oxides, Springer International Publishing, Cham, 2017, pp. 29–58, https://doi.org/.10.1007/7081_2017_3.
[5] G. Bellér, M. Szabó, G. Lente, I. Fábián, J. Org. Chem. 81 (2016) 5345–5353, https://doi.org/10.1021/acs.joc.6b00641.
[6] Ferenc Najóczki, Gábor Bellér, Mária Szabó, I. Fábián, New J. Chem., 41 (2017) 10.1039/C7NJ01860F.
[7] Clifford Owens, Anne Kelly Filo, Julia M. Woods, Louis L. Pytlewski, Anthony N. Speca, N.M. Karayannis, J. Inorg. Nucl. Chem., 43 (1981) 177-180 https://doi.org/10.1016/0022-1902(81)80459-9.
[8] A.N. Speca, N.M. Karayannis, L.L. Pytlewski, Inorg. Chim. Acta 9 (1974) 87–93, https://doi.org/10.1016/S0020-1693(00)89888-6.
[9] A.N. Speca, L.L. Pytlewski, N.M. Karayannis, J. Inorg. Nucl. Chem. 36 (1974) 3751–3761, https://doi.org/10.1016/0022-1902(74)80160-0.
[10] F. Najóczki, M. Szabó, N. Lihi, A. Udvardy, I. Fábián, Molecules 26 (2021) 3632, https://doi.org/10.3390/molecules26123632.
[11] H.M. Irving, M.G. Miles, L.D. Pettit, Anal. Chim. Acta 38 (1967) 475–488, https://doi.org/10.1016/S0003-2670(01)80616-4.
[12] L. Zékány, I. Nagypál, PSEQUAD: a comprehensive program for the evaluation of potentiometric and/or spectrophotometric equilibrium data using analytical derivatives, in: D.J. Leggett (Ed.), Computational Methods for the Determination of Formation Constants, Plenum Press, New York, 1985, pp. 291–353.
[13] P.S. Gans, A. Vacca, J. Chem. Soc. Dalton Trans. 6 (1985) 1195–1200, https://doi.org/10.1039/DT9850001195.
[14] A. Rockenbauer, L. Korecz, Appl. Magn. Reson. 10 (1996) 29–43, https://doi.org/10.1007/BF03163097.
[15] A. Rockenbauer, T. Szabó-Plánka, Z. Árkosi, L. Korecz, J. Am. Chem. Soc. 123 (2001) 7646–7654, https://doi.org/10.1021/ja0102888.
[16] W. Zhai, Y. Feng, H. Liu, A. Rockenbauer, D. Mance, S. Li, Y. Song, M. Baldus, Y. Liu, Chem. Sci. 9 (2018) 4381–4391, https://doi.org/10.1039/C8SC00969D.
[17] L. Farrugia, J. Appl. Cryst. 45 (2012) 849–854, https://doi.org/10.1107/S0021889812029111.
[18] O.V. Dolomanov, L.J. Bourhis, R.J. Gildea, J.A.K. Howard, H. Puschmann, J. Appl. Cryst. 42 (2009) 339–341, https://doi.org/10.1107/S0021889808042726.
[19] A. Altomare, M.C. Burla, M. Camalli, G.L. Cascarano, C. Giacovazzo, A. Guagliardi, A.G.G. Moliterni, G. Polidori, R. Spagna, J. Appl. Cryst. 32 (1999) 115–119, https://doi.org/10.1107/S0021889898007717.
[20] G. Sheldrick, Acta Crystallogr. C 71 (2015) 3–8, https://doi.org/10.1107/S2053229614024218.
[21] A. Spek, Acta Crystallogr. E 76 (2020) 1–11, https://doi.org/10.1107/S2056989019016244.
[22] C.F. Macrae, I.J. Bruno, J.A. Chisholm, P.R. Edgington, P. McCabe, E. Pidcock, L. Rodriguez-Monge, R. Taylor, J. van de Streek, P.A. Wood, J. Appl. Cryst. 41 (2008) 466–470, https://doi.org/10.1107/S0021889807067908.
[23] F. Neese, WIREs Comput. Mol. Sci. 2 (2012) 73–78, https://doi.org/10.1002/wcms.81.
[24] A.D. Becke, J. Chem. Phys. 98 (1993) 5648–5652, https://doi.org/10.1063/1.464913.
[25] C. Lee, W. Yang, R.G. Parr, Phys. Rev. B 37 (1988) 785–789, https://doi.org/10.1103/PhysRevB.37.785.
[26] S. Grimme, J. Antony, S. Ehrlich, H. Krieg, J. Chem. Phys. 132 (2010), 154104, https://doi.org/10.1063/1.3382344.
[27] A.J.H. Wachters, J. Chem. Phys. 52 (1970) 1033–1036, https://doi.org/10.1063/1.1673095.
[28] D.P. Chong, Recent Advances in Density Functional Methods. https://doi.org/.10.1142/2914.

[29] V. Barone, M. Cossi, J. Tomasi, J. Chem. Phys. 107 (1997) 3210–3221, https://doi.org/10.1063/1.474671.
[30] N. Armaroli, L. De Cola, V. Balzani, J.-P. Sauvage, C.O. Dietrich-Buchecker, J.-M. Kern, J. Chem. Soc. Faraday Trans. 88 (1992) 553–556, https://doi.org/10.1039/FT9928800553.
[31] L. Gasque, R. Moreno-Esparza, L. Ruiz-Ramírez, J. Inorg. Biochem. 48 (1992) 121–127, https://doi.org/10.1016/0162-0134(92)80021-M.
[32] Y. Hiroshi, I. Taro, Bull. Chem. Soc. Jpn 39 (1966) 2054, https://doi.org/10.1246/bcsj.39.2054.
[33] H. Irving, D.H. Mellor, J. Chem. Soc. (Resumed) (1962) 5222–5237, https://doi.org/10.1039/JR9620005222.
[34] E. Garribba, G. Micera, D. Sanna, L. Strinna-Erre, Inorg. Chim. Acta 299 (2000) 253–261, https://doi.org/10.1016/S0020-1693(99)00508-3.
[35] I. Fábián, Inorg. Chem. 28 (1989) 3805–3807, https://doi.org/10.1021/ic00319a011.
[36] M. Noack, G. Gordon, J. Chem. Phys. 48 (1968) 2689–2699, https://doi.org/10.1063/1.1669503.
[37] B.F. Hoskins, F.D. Whillans, J. Chem. Soc. Dalton Trans. (1975) 1267–1272, https://doi.org/10.1039/DT9750001267.
[38] I. Fábián, H. Diebler, Inorg. Chem. 26 (1987) 925–928, https://doi.org/10.1021/ic00253a029.
[39] Y.-Q. Zheng, J.-L. Lin, J. Sun, W.-J. Chen, Z. Anorg. Allg. Chem., 626 (2000) 1505-1507 https://doi.org/.10.1002/1521-3749(200007)626:7<1505::AID-ZAAC1505>3.0.CO;2-7.
[40] M.E. Moustafa, P.D. Boyle, R.J. Puddephatt, Organomet. 33 (2014) 5402–5413, https://doi.org/10.1021/om500712e.
[41] J. Kozisek, P. Baran, D. Valigura, Acta Crystallogr. C 48 (1992) 31–33, https://doi.org/10.1107/S0108270191009642.
[42] G. Sciortino, J.-D. Maréchal, I. Fábián, N. Lihi, E. Garribba, J. Inorg. Biochem. 204 (2020), 110953, https://doi.org/10.1016/j.jinorgbio.2019.110953.
[43] A.G. Blackman, E.B. Schenk, R.E. Jelley, E.H. Krenske, L.R. Gahan, Dalton Trans. 49 (2020) 14798–14806, https://doi.org/10.1039/D0DT02985H.
[44] G.R. Newkome, K.J. Theriot, V.K. Gupta, F.R. Fronczek, G.R. Baker, J. Org. Chem. 54 (1989) 1766–1769, https://doi.org/10.1021/jo00268a055.
[45] S.E. Kutyła, D.K. Stępień, K.N. Jarzembska, R. Kamiński, Ł. Dobrzycki, A. Ciesielski, R. Boese, J. Młochowski, M.K. Cyrański, Cryst. Growth Des. 16 (2016) 7037–7050, https://doi.org/10.1021/acs.cgd.6b01250.
[46] N. Hisayoshi, D. Yoshito, Bull. Chem. Soc. Jpn 48 (1975) 2557–2560, https://doi.org/10.1246/bcsj.48.2557.
[47] W.D. Harrison, B.J. Hathaway, Acta Crystallogr. B 35 (1979) 2910–2913, https://doi.org/10.1107/S0567740879010943.
[48] V.F.S. Pape, N.V. May, G.T. Gál, I. Szatmári, F. Szeri, F. Fülöp, G. Szakács, É. A. Enyedy, Dalton Trans. 47 (2018) 17032–17045, https://doi.org/10.1039/C8DT03088J.
[49] M.S. Haddad, S.R. Wilson, D.J. Hodgson, D.N. Hendrickson, J. Am. Chem. Soc. 103 (1981) 384–391, https://doi.org/10.1021/ja00392a024.